A neutron scattering study of strong symmetric hydrogen bonds in potassium and cesium hydrogen bistrifluoroacetates: Determination of the crystal structures and of the single-well potentials for protons

François Fillaux, Alain Cousson, Juan F. R. Archilla, John Tomkinson

A neutron scattering study of strong symmetric hydrogen bonds in potassium and cesium hydrogen bistrifluoroacetates: Determination of the crystal structures and of the single-well potentials for protons

François Fillaux*†

LADIR-CNRS, UMR 7075 Université P. et M. Curie,

2 rue Henry Dunant, 94320 Thiais, France

Alain Cousson‡

Laboratoire Léon Brillouin (CEA-CNRS),

C.E. Saclay, 91191 Gif-sur-Yvette, cedex, France

Juan F R Archilla§

Group of Nonlinear Physics, Departamento de Física Aplicada I,

ETSI Informática. Avda Reina Mercedes s/n, 41012-Sevilla, Spain

John Tomkinson¶

Rutherford Appleton Laboratory, Chilton,

Didcot, OX11 0QX, United Kingdom

(Dated: April 22, 2008)

* Corresponding author
homepage http://ulysse.glvt-cnrs.fr/ladir/pagefillaux.htm

Abstract

The crystal structures of potassium and cesium bistrifluoroacetates, $KH(CF_3COO)_2$ and $CsH(CF_3COO)_2$, respectively, were determined at room and cryogenic temperatures with the single crystal neutron diffraction technique. The crystals belong to the monoclinic space groups, $I2/a$ and $A2/a$, respectively, and there is no evidence of any structural phase transition. In both crystals, trifluoroacetate entities in centrosymmetric dimers are linked by very short hydrogen bonds lying across a center of inversion. The thermal parameters provide no evidence of any double minimum potential for hydrogen bond protons. Single-minimum potentials were determined via best fitting to the inelastic neutron scattering spectral profiles of the stretching vibrations. They comprise a narrow well for the ground state and a very broad quasi-harmonic well for excited states. The spread out of the wave functions of these states shows that protons are no longer confined between the oxygens. Presumably, they are attracted by the lone-pairs of oxygen atoms. These potential emphasize the covalent nature of the OO bond and the ionic character of the hydrogen bond proton.

Keywords: Single crystals neutron diffraction, inelastic neutron scattering, hydrogen bond, proton dynamics

I. INTRODUCTION

Hydrogen bonds are ubiquitous in Nature, so the concept of hydrogen bonding is of fundamental importance in many disciplines across physics, chemistry, and biology. However, there are many unresolved problems about the quantum nature of this particular chemical bond.[1–5] The enormous range of energy, from about 2 to 40 kcal mol^{-1}, may be part of the difficulty, for hydrogen bonds might be not amenable to a single concept. In particular, current controversies are focussed on very strong hydrogen bonds OHO (VSHB) whose lengths are shorter than ≈ 2.45 Å.[6–10] These bonds exhibit exceptional physical and chemical properties. In addition, the possible role of VSHB's in enzymatic catalysis broadens their potential significance.[11–18] The purpose of this present paper is to enlighten on some structural and dynamical features of these bonds.

It is a widespread opinion that structural,[7–10] dynamical,[19] and magnetic[16,20–22] properties of VSHB's in crystals are inconsistent with the relatively long-range attraction, predominantly electrostatic in nature, attributed to weak hydrogen bonds. Gilli et al.,[8–10] or Tian and Li,[23] have suggested a resonance between covalent structures (e.g., O—H$\cdots$O $\longleftrightarrow$ O$\cdots$H—O), but Sørensen et al.[24] have opposed a counterexample to this view.

From the dynamical viewpoint, one can distinguish "single well hydrogen bonds" (SWHB) and "low barrier hydrogen bonds" (LBHB),[12–14,21,22] depending on the shape of the potential for protons moving along the O$\cdots$O direction. (In the present paper, this coordinate is x_a and the eigen state vector $|x_a\rangle_n$ is at $h\nu_{an}$.) These potentials could explain different chemical reactivities, for example isotopic fractionation factors,[21] but experimental or theoretical evidences are rather scarce.

The prototypical intramolecular strong-symmetric hydrogen bond (SSHB) in the crystal of potassium hydrogen maleate, KH(OOC-CH=CH-COO), or KHM, has been thoroughly investigated with X-ray or neutron diffraction,[25–27] infrared and Raman,[28–31] inelastic neutron scattering (INS),[27,32–34] NMR,[35,36] and calorimetry.[37] The linear hydrogen bond is very short ($R_{\mathrm{OO}} = 2.427(1)$ Å at 5 K) and crystallographically symmetrical. The probability density of the hydrogen bond proton located at the center, visualized as a thermal ellipsoid, accords with a single-well. INS spectra of single-crystals of various H/D derivatives have revealed a large number of $|x_a\rangle_n$ states (at least 7 between 500 and 1300 cm^{-1}) consistent with a symmetric funnel-shaped potential (Fig. 1). To the best of our knowledge, this

potential has never been confronted with theoretical quantum chemistry, so the interpretation is circumstantial. Wilson et al.,[38] using plane-wave density functional theory, have calculated the potential energy in this crystal, but only for a very limited range of proton displacements ($\Delta x_a \approx \pm 0.1$ Å) that cannot make any contact with the funnel shape.[39] On the other hand, calculations of the isolated maleate ion lead to a LBHB at variance with the crystal structure.[38,40,41] We are not aware of any theoretical modelling of very large proton displacements (~ 2 Å) for KHM in the crystal field.

To the best of our knowledge, the funnel-potential of KHM is unique. Could it be of general relevance to SSHB's? That is the question at issue in this present paper. This question is controversial since a new intramolecular VSHB ($R_{\mathrm{OO}} = 2.388(5)$ Å at 20 K) has been reported in the crystal of 4-cyano-2,2,6,6-tetramethyl-3,5-heptanedione (4CTH).[22] In contrast to KHM, the hydrogen bond is not linear ($r_{\mathrm{OH}} \approx 1.22$ Å, $\widehat{\mathrm{OHO}} \approx 157°$) and, needless to say, non centrosymmetric. An INS band at 371 cm^{-1}, tentatively assigned to $|x_a\rangle_1$, along with solid-state NMR measurements, were regarded as possible evidences of a LBHB. However, there are solid counterarguments to this conclusion. (i) These authors point out that "the neutron [diffraction] data better fit a single anisotropic thermal ellipsoid...", so a single-well is more plausible, even though the academic case of a potential barrier below the zero-point energy cannot be excluded. (ii) The same authors report that ab initio calculations of the isolated molecule lead to an imaginary frequency suggesting a potential barrier at the center. However, such calculations are not conclusive. For example, they lead to a LBHB for the isolated maleate ring that is at variance with the SWHB observed in the crystal. One cannot exclude the important role of the crystal field in the calculation of the optimized geometry. In addition, spectroscopic observables are representative of an effective potential that can be different from the Born-Oppenheimer potential. (iii) The INS spectra were measured only below 640 cm^{-1}, so it is unknown whether higher transitions corroborate a double-well. (iv) Even for the methyl deuterated derivative, the neutron flux scattered by all atoms is much greater than that scattered by the single hydrogen bond proton, so the contrast of intensities is not sufficient to establishing an assignment scheme. (v) The invaluable information provided by infrared and Raman is missing. These numerous drawbacks show that the band assignment and the double-well proposed by these authors deserve reservations. Furthermore, it is widely accepted that the potential barrier and the hydrogen bond length should decrease simultaneously. A double-well for a hydrogen

bond shorter than that in KHM would be therefore rather odd, unless it would be due to the nonlinear OHO geometry. Unfortunately, the large number of tetramethyl groups is a serious hurdle for further INS studies of this interesting system.

In the present paper, in order to fully exploit the contrast of intensities for infrared, Raman, and INS, we consider crystals in which hydrogen bond protons are singled out. Potassium, or cesium, hydrogen bistrifluoroacetate, $KH(CF_3COO)_2$, (KTFA), or $CsH(CF_3COO)_2$, (CTFA), are known examples of "intermolecular" SSHB's.[42] At room temperature, trifluoroacetate dimers, $H(CF_3COO)_2^-$, are linked by crystallographically symmetric hydrogen bonds with $R_{OO} = 2.435(7)$ Å or 2.38(3) Å, respectively. The vibrational spectra of these salts at a very low temperature[19,43,44] evidence several $|x_a\rangle_n$ states in the same frequency range as for KHM (500-1100 cm^{-1}), but with quite different profiles of intensity. In a previous work,[44] it was suggested that CTFA could be a LBHB case, but there is no neutron diffraction data to support this proposal. We report below single-crystal neutron diffraction measurements consistent with single-wells for protons at any temperature. This result prompts us to revisit the vibrational spectra and we propose a funnel-potential largely inspired by that shown in Fig. 1, but not quite the same. We tentatively rationalize these various potentials with bare protons $H^{\oplus}$ weakly bound to $^{\ominus}O$——$O^{\ominus}$ bonds.

This paper is organized as follows. The crystal structures at room and cryogenic temperatures are presented in Section II. In Section III, we propose an assignment scheme for the $|x_a\rangle_n$ states based on infrared, Raman and INS spectra. In Section IV, we elaborate on the theoretical framework for proton dynamics, we determine the best potential, and we examine some consequences to the quantum nature of SSHB's.

II. CRYSTAL STRUCTURES

Single crystals were obtained by slow crystallization from aqueous solutions. Approximately cubic samples ($3 \times 3 \times 3$ mm^3) were loaded into aluminum containers and then mounted in a cryostat. Measurements (see Table I) were carried out with the Stoe four-circle diffractometer 5C2 at the Orphée reactor (Laboratoire Léon-Brillouin).[45] Data analysis was carried out with the computer package CRYSTALS.[46,47] Absorption corrections were ignored.

The structures at room temperature are similar to those previously determined with X-

rays.[42] At low temperatures, the lattice parameters (Table I) and the positional parameters (Tables II and III) are not significantly changed. There is no evidence of any phase transition or proton disorder. The potassium and cesium salts belong to the $I2/a$ and $A2/a$ monoclinic space groups, respectively, both with four dimer entities in the unit cell. The crystallographically equivalent TFA's of a dimer are linked by short linear hydrogen bonds lying across a center of inversion (Figs 2 and 3) The conformations of the TFA entities are quite different for the two salts: a C—F bond is *trans* to the C2O2 bond for KTFA, while a C—F bond is perpendicular to the carboxylic plane for CTFA. At room temperature, all temperature factors increase substantially (see Table IV, Fig. 2, and Table V, Fig. 3). They are 10-15 times greater for heavy atoms and only 3-5 times greater for protons. For heavy atoms, the ellipsoids suggest librations around the C—C bonds.

Hydrogen bond lengths are identical at low temperature, $R_{\rm OO} = 2.436(3)$ Å for KTFA or 2.436(4) Å for CTFA, and very close to $R_{\rm OO} = 2.427(1)$ Å for KHM. Differences of about twice the variance are not significant. These SSHB's are therefore unaffected by the crystal stacking, or the TFA conformation, or resonance within the maleate ring. At room temperature, $R_{\rm OO} = 2.432(3)$ Å for KTFA and 2.444(2) Å for CTFA. These temperature effects are not significant, compared to the estimated variances. The difference between the two salts is smaller than that previously determined with X-rays.[42] This is likely a consequence of the huge X-ray cross-section of Cs atoms.

There is no evidence of any splitting of the proton sites that could suggest a double-well and the thermal factors at low temperatures are consistent with a quasi-harmonic single-well for the ground state. Supposing an oscillator mass of 1 amu (see below Sec. IV), the mean-square amplitudes for the three proton modes at frequencies about 800 cm^{-1} (ν_a), 1250 cm^{-1} (out-of-plane bending, γ), and 1600 cm^{-1} (in-plane bending, δ),[44] are $u^2_{0\nu} \approx 0.021$ Å^2, $u^2_{0\gamma} \approx 0.013$ Å^2, $u^2_{0\delta} \approx 0.010$ Å^2. The averaged value $\langle u^2_0 \rangle \approx 0.015$ Å^2 compares to the thermal factors U(iso) = 0.0166 Å^2 in Tables II and III, or, equivalently, to the averaged anisotropic factors $U = (U_{11} + U_{22} + U_{33})/3 \approx 0.017$ Å^2 in Tables IV and V. The difference $U - \langle u^2_0 \rangle \approx 0.002$ Å^2 is similar to the thermal parameters for oxygen atoms. There is no evidence of any double-well.

It is noticeable that the thermal factors for protons at room temperature are very close to the sum of the thermal factors determined at low temperature and those for O atoms at room temperature. Figs 2 and 3 show that the thermal ellipsoids for O atoms are very

small at low temperatures, compared to those for protons, while at room temperature the thermal ellipsoids for protons and oxygens are similar. This suggests that the mean-square amplitudes for protons are largely temperature independent and temperature effects arise from primarily convolution with the probability density of O atoms. This is consistent with rather deep wells for protons, such that the populations of excited states remain negligible at room temperature. There is therefore no evidence of any double-well, even at room temperature. On the other hand, the thermal population of phonons at low frequencies should account for the increase of the thermal factors of heavy atoms at room temperature.

III. INS BAND PROFILES

INS band intensities are proportional to the nuclear cross-sections for incoherent scattering, on the one hand, and to the scattering function, on the other.[48] The incoherent cross-section is rather large for protons ($\sigma_H \approx 80$ b) and negligibly small for all other nuclei under consideration. The scattering function $S(\mathbf{Q}, \nu)$ depends on the neutron momentum transfer vector $\mathbf{Q} = \mathbf{k}_0 - \mathbf{k}_f$, defined by the initial, $\mathbf{k}_0$, and the final, $\mathbf{k}_f$, wave vectors, and on the energy transfer $h\nu$. With the TFXA-spectrometer utilized in Ref. [44], only scattering events corresponding to the maximum of the scattering function for harmonic bare protons are counted (see Appendix).

The previously reported INS spectra of the two salts are very similar.[44] The γH modes give narrow single bands at ≈ 1225 cm^{-1} (KTFA) or ≈ 1260 (CTFA) and overtones at ≈ 2450 cm^{-1} (KTFA) or ≈ 2515 cm^{-1} (CTFA), consistent with quasi-harmonic oscillators. The intensity ratios $I_{0\longrightarrow 2}/I_{0\longrightarrow 1}$ accord with an oscillator mass of ≈ 1 amu. The full widths at half maximum (FWHM) of ≈ 50 cm^{-1} are representative of the density-of-states, convoluted with the spectrometer resolution ($\Delta\nu/\nu \approx 0.02$) that is $\Delta\nu \approx 25$ cm^{-1} at 1250 cm^{-1}. The upper bound for the frequency dispersion (FWHM $-\Delta\nu \approx 25$ cm^{-1}) accords with rather small coupling terms between protons. Similarly, the δH modes show single bands at ≈ 1600 cm^{-1} (FWHM ≈ 70 cm^{-1}) for both salts. For KTFA, the weak overtone at ≈ 3200 cm^{-1} is also consistent with a quasi-harmonic oscillator with $m \approx 1$ amu. (The overtone is not clearly observed for CTFA, presumably because of larger statistical errors.)

In marked contrast to the bending modes, the stretching show broad profiles, composed of partially resolved sub-bands between 500 and 1100 cm^{-1}, which cannot be rationalized with

a quasi-harmonic model (see Fig. 4). Tentative decompositions with gaussian components are very similar for the two salts (Fig. 4 and Table VI). Only one component at ≈ 850 cm^{-1} for CTFA is not visible for KTFA. Such similar profiles for quite different crystal structures suggest that the crystal-field is not the main band splitting factor. Further information can be sorted out of the Infrared and Raman spectra.

In the infrared, the γH's are rather weak and the δH's are practically invisible. The spectra are dominated by narrow bands, due to TFA entities, superimposed to the very broad stretching profiles. The maxima of intensity at $\approx$ 800 cm^{-1} coincide with those observed with INS. Above 1000 cm^{-1}, there are long tails of continuous intensity, extending up to at least 2000 cm^{-1}, which are not observed with INS. The broader profiles observed in the infrared, at the Brillouin-zone center, compared to INS, for the whole density-of-states, confirm that dispersion is not the main band shaping mechanism. In fact, weak dynamical coupling is in line with the rather large proton-proton distances in the crystals. (The shortest distances are 4.34 Å for KTFA and 6.72 Å for CTFA.)

The Raman spectra are exclusively due to the TFA entities, while proton modes are invisible. For KTFA, the strong Raman bands at 850-854 cm^{-1}, analogous to that observed for CTFA,[44] suggest that the INS counterpart should exist, although it is not resolved.

The assignment scheme in Table VII, is based on the contrast of intensities measured with INS, infrared and Raman. (The dubious component above 1000 cm^{-1} is ignored.) INS components visible in Raman are assigned to TFA modes acquiring INS intensity via resonance with proton states (see below). The other sub-bands are associated with $|\nu_a\rangle_n$ states. Owing to the spectrometer resolution ranging from $\approx$ 10 to 20 cm^{-1}, the intrinsic bandwidths should be much less than the FWHM's in Table VII. Such narrow components are consistent with long-live stationary states.

IV. PROTON DYNAMICS

Within the framework of the Born-Oppenheimer approximation, the vibrational Hamiltonian can be partitioned as

$$\mathcal{H}_{\rm v} = \mathcal{H}_{\rm H} + \mathcal{H}_{\rm at} + \mathcal{C}_{\rm Hat}, \tag{1}$$

where $\mathcal{H}_{\rm H}$ and $\mathcal{H}_{\rm at}$ represent protons ($H^{\oplus}$) and heavy atoms, respectively, while $\mathcal{C}_{\rm Hat}$ couples the subsystems. For OHO hydrogen bonds, the dominant coupling term between $\nu_{\rm OH}$

and $\nu_{\rm OO}$ can be evaluated from the slope $S = \Delta\nu_{\rm OH}/\Delta R_{\rm OO}$ of the empirical correlation $\nu_{\rm OH}(R_{\rm OO})$.[10,19] According to Novak,[19] the slope increases continuously as $R_{\rm OO}$ decreases: $S \approx 1500$ cm^{-1}Å^{-1} for weak hydrogen bonds ($R_{\rm OO} > 2.7$ Å); $S \approx 5000$ cm^{-1}Å^{-1} for intermediate hydrogen bonds ($R_{\rm OO} \approx 2.6 - 2.7$ Å); $S \approx 12000$ cm^{-1}Å^{-1} for strong hydrogen bonds ($R_{\rm OO} < 2.6$ Å). This strong coupling is widely recognized as an important band shaping factor.[3,49–52]

However, we argue that the slope for strong hydrogen bonds should not be extrapolated for VSHB's without caution because there is no known example of hydrogen bonds with $R_{\rm OO}$ significantly shorter than ≈ 2.4 Å and stretching frequency much lower than ≈ 500 cm^{-1}. [For the time being, we put aside the dubious assignment at 371 cm^{-1} for 4CTH[22] (see above).] We posit that the stretching frequency reaches a minimum value for VSHB's like those in TFA's or KHM, so the leading coupling term in (1) vanishes ($S \approx 0$) and proton dynamics are only weakly coupled to oxygen atoms. In the zeroth-order approximation, the spectral profile is representative of the potential function along the stretching coordinate, say $\mathcal{V}(x_a)$, and weak coupling terms with other degrees of freedom can be treated as perturbations. (Note that the potential function for KHM was determined on this basis.[27])

A. Resonance

Weak coupling terms account for INS intensities of the otherwise invisible TFA modes. Within the framework of the adiabatic separation of $\mathcal{H}_{\rm H}$ and $\mathcal{H}_{\rm at}$[53,54] the ground-state vector can be written as

$$|x_a\rangle_0|y\rangle_0|z\rangle_0 \bigotimes_i |X_i\rangle_0|Y_i\rangle_0|Z_i\rangle_0, \tag{2}$$

where x_a, y, z are proton coordinates, while X_i, Y_i, Z_i, are normal coordinates for heavy atoms. When an excited proton state, say $|x_a\rangle_n$, is close enough to a heavy atom state, $|A_i\rangle_{Ni}$ ($A_i = X_i, Y_i, Z_i$), weak coupling terms lead to state mixing (resonance). Within the framework of first order perturbation theory, the energies of the uncoupled states are shifted apart and the mixed vector states can be written as

$$\begin{aligned} |1\rangle &= \alpha|x_a\rangle_n + \beta|A_i\rangle_{Ni}, \\ |2\rangle &= -\beta|x_a\rangle_n + \alpha|A_i\rangle_{Ni}, \end{aligned} \tag{3}$$

with $\alpha^2 + \beta^2 = 1$. The INS intensity of the transition to the unperturbed state, $|x_a\rangle_0 \longrightarrow |x_a\rangle_n$, is distributed among transitions $|x_a\rangle_0 \longrightarrow |1\rangle$ and $|x_a\rangle_0 \longrightarrow |2\rangle$ with relative intensities

proportional to α^2 and β^2, respectively. Such resonances are more likely to occur among the numerous $|x_a\rangle_n$ states than with the quasi harmonic bending states. In addition, more than two states can be eventually mixted, but we do not need to elaborate any further, as our purpose is limited to a qualitative interpretation.

The INS intensities of the components at 527 and 559 cm^{-1} in Table VI are thus attributed to resonances with TFA modes. These intensities are added to the $0 \longrightarrow 1$ transition (Table VII) and the resonance induced frequency shift is neglected. Similarly, the intensity of the $0 \longrightarrow 2$ transition is the sum of intensities for components $4, 5, 6$. This grouping is likely not unique and possible resonances with other TFA modes below 500 cm^{-1} are ignored. This leads to unavoidable uncertainties for relative intensities and unperturbed levels. A very similar assignment scheme could be proposed for CTFA.

B. Potential function

By analogy with the funnel-shaped potential of KHM, $\mathcal{V}(x_a)$ (Fig. 5) is represented with a narrow gaussian well, imposed by the $0 \longrightarrow 1$ transition at 601 cm^{-1}, and a broad quasi harmonic potential, shifted off-center, consistent with the energy-level spacing ($\lessapprox 100$ cm^{-1}) for higher excited states and with the observed relative intensities as:

$$\mathcal{V}(x_a) = -ax_a + bx_a^2 - cx_a^3 - d\exp(-fx_a^2). \tag{4}$$

In addition to the gaussian and harmonic wells, the linear term is crucial to adjusting relative intensities, and the cubic term accounts for anharmonic corrections to the upper energy levels. For the sake of definiteness, the number of parameters is set equal to the number of observed transitions. Note that this model potential cannot account for the continuum of infrared intensity that could be due to unbound states.

Eigen states were calculated with the variational method (see Appendix) and the coefficients were adjusted via least square fitting exercises. The maximum deviation of $\approx 2\%$ (Table VII) is comparable to the spectrometer resolution and within the bandwidths. The calculated intensities are in qualitative agreement with observations, so the eigen functions should be reasonably well calculated. Needless to say, the potential shape is imposed by the assignment scheme, so additional terms in (4), or alternative grouping of intensities, or minor corrections for the unperturbed levels should be of no consequence to the overall

shape.

C. Discussion

The wave function in the ground state is practically symmetrical with respect to the center, in accordance with the crystal structure. In addition, the mean square amplitude (the variance of the gaussian-like squared wave function, $u_{0a}^2 \approx 0.02$ Å^2) is comparable to the thermal parameters at low temperatures (Table IV). It is worthy of note that a double-well with a barrier height below the ground state would increase u_{0a}^2 beyond the limit imposed by the thermal factor. At room temperature, the population of excited states ($\approx 5\%$) should give a diffuse probability density too weak to be visible with the precision of neutron diffraction.

In the excited states, the spatial extension of the wave functions is much greater than R_{OO}, so the proton is no longer confined between the O atoms. For KHM, it was speculated that the hydrogen bond could be broken at a rather modest energy cost, thanks to the internal strain of the ring.[27] However, this view was not confirmed with DFT calculations.[23] Furthermore, there is no internal strain for intermolecular SSHB's, so this option must be abandoned.

Upon the assumption that the bond is not broken by vibrational excitations, the mean position $\langle x_a^2 \rangle^{\frac{1}{2}} \approx 1$ Å in the excited states of KTFA suggests that the proton is localized around one of the two oxygens. It seems to be weakly bound to the lone-pairs via the overlap between vibrational wave functions and electron orbitals. Similarly, the delocalized wave functions in the upper symmetrical well of KHM (Fig. 1) could overlap the lone-pairs of the two oxygens. The schemes presented in Fig. 6 suggest a correlation between the potential asymmetry/symmetry and the spatial orientation of the lone-pairs. For intermolecular hydrogen bonds, lone pairs pointing to opposite directions lead to localization of the excited proton states around either of the two oxygens, hence an asymmetric potential. Alternatively, lone-pairs in the plane of the maleate ring lead to delocalization over the two oxygens and a symmetric potential.

If oxygens are thought of as hard spheres, the spread out of the wave functions along x_a is possible if large displacements occur simultaneously perpendicular to the OO direction. Vibrational spectra do not provide any definite information on such displacements, except

that there is no evidence of any rotation of the proton coordinates in the excited states. Otherwise, one should observe some mixing of the stretching and bending modes. Theoretical modelling should consider very large proton displacements in multi dimensions.

In the ground state, hydrogen bonds can be conceived of as bare protons sitting at the center: $^{\ominus}$O—H$^{\oplus}$—O$^{\ominus}$. The binding energy of H$^{\oplus}$ to the local maximum of the density of negative charges corresponds to the depth of the central well minus the zero-point energy, namely ≈ 600 cm^{-1} for TFA's or ≈ 500 cm^{-1} for KHM. They are marginal compared to the total hydrogen bond energy. This ionic scheme is at variance with the resonance O—H$\cdots$O$^{\ominus}$ $\longleftrightarrow$ $^{\ominus}$O$\cdots$H—O advocated by Gilli et al. in order to stress the covalent character of the OH bond.[8,23]

For the sake of preserving the center of symmetry, excited vibrational states of the TFA's must be represented by mixtures, with equal probabilities, of non-overlapping degenerate states $|^{\ominus}\mathrm{O}\text{——}\mathrm{O}^{\ominus}\mathrm{H}^{\oplus}\rangle_n$ and $|^{\oplus}\mathrm{H}^{\ominus}\mathrm{O}\text{——}\mathrm{O}^{\ominus}\rangle_n$, located on either sides of the OO bond (Fig. 6). These states can be thought of as "localized proton orbitals". For KHM, excited vibrational states are represented by symmetric and antisymmetric superposition states, $2^{-1/2}[|^{\ominus}\mathrm{O}\text{——}\mathrm{O}^{\ominus}\mathrm{H}^{\oplus}\rangle \pm |^{\oplus}\mathrm{H}^{\ominus}\mathrm{O}\text{——}\mathrm{O}^{\ominus}\rangle]$, arising from the overlap between the localized orbitals. These states can be termed "delocalized proton orbitals". The rather small $|1\rangle - |2\rangle$ splitting of 30 cm^{-1} in Fig. 1, compared to the mean level spacing greater than 100 cm^{-1}, suggests proton "tunnelling" between the shallow minima created by lone-pairs. It is not clear as to whether these delocalized states contribute to the binding energy. In any case, this contribution should be marginal.

In the excited states, the charge compensating proton is apparently no longer involved in the bonding, so we speculate that the "bare" $^{\ominus}$O——O$^{\ominus}$ bond is intrinsically stable. To suppose it be covalent in nature is not irrelevant since binding energies for SSHB's are on the scale of those for peroxides (O–O ≈ 1.48 Å), found in the range $45 - 35$ kcal.mol^{-1}.[55] Needless to say, this comparison is not a proof that $^{\ominus}$O——O$^{\ominus}$ bonds are the longest covalent bonds ever known. This interpretation deserves further theoretical investigations.

The funnel potentials suggest that the total binding energy can be partitioned in two parts: the binding energy for protons, the "hydrogen bonding" contribution, and the "covalent bonding" energy for the bare $^{\ominus}$O——O$^{\ominus}$ bond. Accordingly, SSHB are essentially covalent bonds, with a marginal hydrogen bond character. If we suppose that for shorter R_{OO}'s the binding energy of H$^{\oplus}$ vanishes, then SSHB's should be close to the physical limit

for the existence of hydrogen bonds. Conversely, we extrapolate that as R_{OO} increases, the hydrogen bond character increases while the covalent bonding decreases, so that the total binding energy decreases. For the sake of continuity near the dissociation threshold, the O$\cdots$H–O scheme emphasizing the covalent nature of the OH bond and long-range dipolar interactions should supersede the "ionic" scheme.

Conclusion

Very short hydrogen bonds linking trifluoroacetate entities in crystals are symmetrical at room and cryogenic temperatures. The thermal ellipsoids exclude a double-well for protons, within the limitations imposed by quantum mechanics. The contrasts of intensities (infrared, Raman and INS) allow us to establishing an assignment scheme for the spectral profiles.

We argue that bond lengths and proton stretching frequencies of strong symmetric hydrogen bonds are close to the lower bounds at which the main coupling term between proton and oxygen atoms goes to zero. Proton dynamics are largely insulated from the lattice and weak coupling terms can be treated as perturbations. Vibrational spectra are consistent with funnel-shaped potentials that could be distinctive of very strong hydrogen bonds. Protons in excited vibrational states are delocalized over the lone-pairs of oxygen atoms. These states suggest a marked covalent character of $O^{\ominus}$——$O^{\ominus}$ bonds and weak electrostatic interaction with the ionic proton.

Potential functions consistent with energy levels, profiles of intensity, and thermal ellipsoids, are over determined. They enlighten on unforeseen dynamics and electronic structures suggesting that there is not yet a clear understanding of the nature of the hydrogen bond at the fundamental level of quantum mechanics. We propose a comprehensive rationale accounting for similarities (funnel potentials) and differences (symmetry/asymmetry) of the three best studied strong symmetric hydrogen bonds. However, the adequacy of a model to observations, as good as it can be, is not a definite proof that this model is unique. The interpretation advocated in this work should be confronted with complementary experiments, for example solid-state NMR, and theoretical investigations.

Appendix: Calculation of energy levels, wave functions and INS intensities

The variational method is appropriate to determine analytical potential functions fitting any given energy level scheme. The expansion of the eigen functions with harmonic basis sets allows us to calculate all matrix elements of interest for vibrational spectroscopy. In this appendix we gather the formulae to resolve the Schrödinger equation for a dimensionless particle with mass m experiencing a potential $V(x)$ along the x coordinate:

$$-\frac{\hbar^2}{2\,m}\frac{\mathrm{d}^2\Psi}{\mathrm{d}\,x^2} + V(x)\,\Psi = E\,\Psi \tag{5}$$

with

$$V(x) = V_p(x) + V_G(x) = \sum_{l=1}^{6} v_l\,x^l + \sum_{l=1}^{3} a_l \exp(-b_l\,x^2)\,, \tag{6}$$

where V_p is polynomial and V_G is the sum of three gaussians, to allow for a rich variety of potential shapes. We also propose a straightforward method to test the accuracy of the eigenfunctions.

In order to construct a basis set, let $\nu_0 = \omega_0/(2\pi)$ be a frequency and consider the dimensionless variables $\xi = \alpha\,x$, with $\alpha = \sqrt{m\,\omega_0/\hbar}$, $\tilde{V} = V/(\hbar\,\omega_0)$ and $\tilde{E} = E/(\hbar\,\omega_0)$. Then

$$\tilde{V_p} = \sum_{l=1}^{6} \tilde{v}_l\,\xi^l, \tag{7}$$

with

$$\tilde{v}_l = v_l/(\hbar\,\omega_0\,\alpha^l) \tag{8}$$

Here, the scaled energies are such that the level spacing of the harmonic oscillator is 1 instead of 4 in Ref. [56]. The coefficients v_l, divided by a factor of 2 compared to Ref. [56], are such that the potential energy of the harmonic oscillator $\tilde{V} = \xi^2/2$ corresponds to $\tilde{v}_l = 1/2\,\delta_{l,2}$ (where $\delta_{l,2}$ is the Kronecker symbol). Then, $\alpha = \alpha_0\,\sqrt{\tilde{\nu}_0\,m}$ can be expressed in Å^{-1} units with $\alpha_0 = 0.17273$ and $\tilde{\nu}_0 = \omega_0/(2\,\pi\,c)$ in cm^{-1} units.

In the new variables Eq. (5) reads:

$$\hat{h}\,\psi = -\frac{1}{2}\frac{\mathrm{d}^2\psi}{\mathrm{d}\,\xi^2} + \tilde{V}\,\psi = \tilde{E}\,\psi\,, \tag{9}$$

with $\psi = \sqrt{\alpha}\,\Psi$ normalized with respect to ξ. For a harmonic oscillator the normalized solutions of (9) are:

$$u_n(\xi) = (2^n\,n!\sqrt{\pi})^{-1/2}\,H_n(\xi)\exp(-\xi^2/2) \qquad n = 0, 1, \ldots\,, \tag{10}$$

$\{H_n\}$ being the Hermite polynomials. The functions $\{u_n\}$ form a suitable orthonormal basis set for bound states. For numerical calculations the dimension N of the basis has to be finite. We found $N = 60$ is suitable to calculate the 10 lowest energy levels with good accuracy (see below). The matrix elements of $\hat{h}$ in (9) are:

$$\hat{h}_{n,m} = \langle n|\hat{h}|m\rangle = \int_{-\infty}^{\infty} u_n(\xi)\hat{h}\, u_m(\xi)\,\mathrm{d}\,\xi\,. \tag{11}$$

The matrix elements for a sixth order polynomial potential or a gaussian potential can be found in Refs. [56] and [57], respectively. With the alternative definition of the scaling factors, the algorithms for the polynomial form are:

$$\begin{aligned}
\hat{h}^p_{n,n} &= (n+\tfrac{1}{2})\,(\tfrac{1}{2}+\tilde{v}_2) + \tfrac{3}{4}\,(2\,n^2+2\,n+1)\,\tilde{v}_4 \\
&+ \tfrac{1}{8}\,(20\,n^3+30\,n^2+40\,n+15)\,\tilde{v}_6\;; \\
\hat{h}^p_{n,n-1} &= \tfrac{1}{2}\sqrt{2\,n}\,\Big(\tilde{v}_1+\tfrac{3}{2}\,n\,\tilde{v}_3+\tfrac{5}{4}\,(2\,n^2+1)\,\tilde{v}_5\Big)\;; \\
\hat{h}^p_{n,n-2} &= \tfrac{1}{2}\sqrt{n\,(n-1)}\,\Big(-\tfrac{1}{2}+\tilde{v}_2+(2\,n-1)\,\tilde{v}_4 \\
&+ \tfrac{15}{4}\,(n^2-n-1)\,\tilde{v}_6\Big)\;; \\
\hat{h}^p_{n,n-3} &= \tfrac{1}{2}\sqrt{\frac{n\,(n-1)\,(n-2)}{2}}\,\Big(\tilde{v}_3+\tfrac{5}{2}\,(n-1)\,\tilde{v}_5\Big)\;; \\
\hat{h}^p_{n,n-4} &= \tfrac{1}{4}\,\sqrt{n\,(n-1)\,(n-2)\,(n-3)}\,\Big(\tilde{v}_4+\tfrac{3}{4}\,(2\,n-3)\,\tilde{v}_6\Big)\;; \\
\hat{h}^p_{n,n-5} &= \tfrac{1}{4}\,\sqrt{\frac{n\,(n-1)\,(n-2)\,(n-3)\,(n-4)}{2}}\;\tilde{v}_5\;; \\
\hat{h}^p_{n,n-6} &= \tfrac{1}{8}\,\sqrt{n\,(n-1)\,(n-2)\,(n-3)\,(n-4)\,(n-5)}\;\tilde{v}_6\;.
\end{aligned}$$

All other matrix elements are zero except the symmetric ones: $\hat{h}^p_{n-l,n} = \hat{h}^p_{n,n-l}$, $l = 1,\ldots,6$.

For the gaussian potential $W = a\,\exp(-b\,x^2)$, the scaled potential is $\tilde{W} = \tilde{a}\,\exp(-\tilde{b}\,\xi^2)$, with $\tilde{a} = a/(\hbar\,\omega_0)$ and $\tilde{b} = b/\alpha^2$. Matrix elements $\hat{W}_{n,m}$ in the subset $\{u_n\}_{n=0}^{N-1}$ are calculated according to Ref. [57]. The first row of a $(N, 2N-1)$ auxiliary matrix $\hat{G}$ is

$$\hat{G}_{0,m} = \sqrt{\frac{m!}{2^m(1+\tilde{b})}}\,\frac{(-\theta)^{m/2}}{(m/2)!} \quad \text{for m (even)=0,\ldots, 2N-1}\;,$$

with $\theta = \tilde{b}/(1+\tilde{b})$. The second row is:

$$\hat{G}_{1,m} = \sqrt{m}\,\hat{G}_{0,m-1} + \sqrt{m+1}\,\hat{G}_{0,m+1} \quad ;\text{for m (odd)=1,\ldots,2N-2.}$$

Each successive row of index n $(2 \leqq n \leqq N-1)$ depends on the two previous ones as:

$$\begin{aligned}
\hat{G}_{n,m} &= 1/\sqrt{n}\,(\sqrt{m}\,\hat{G}_{n-1,m-1} + \sqrt{m+1}\,\hat{G}_{n-1,m+1} - \sqrt{n-1}\,\hat{G}_{n-2,m}); \\
m &= n, n+2, n+4, \ldots, 2N-n-1
\end{aligned} \tag{12}$$

All elements not explicitly assigned are set to zero. Let us redefine $\hat{G}$ as the (N, N) square matrix corresponding to its first N columns. The procedure above has led to an upper triangular matrix. The elements of the lower triangle are obtained by symmetry $\hat{G}(n, m) = \hat{G}(m, n)$, for all n, m such that $m < n$. The (N, N) matrix corresponding to $\tilde{W}$ is $\hat{W} = \tilde{a}\,\hat{G}(\tilde{b})$, so the matrix $\hat{h}$ for the full potential (6) is:

$$\hat{h} = \hat{h}^p + \sum_{l=1}^{3} \tilde{a}_l\,\hat{G}(\tilde{b}_l). \tag{13}$$

If $\{\tilde{E}_n\}_{n=0}^{N-1}$ are eigenvalues in increasing order, and $\hat{C}$ is the (N, N) matrix whose column n is the normalized eigenvector corresponding to $\tilde{E}_n$, the eigenfunctions are

$$\psi_n(\xi) = \sum_{m=0}^{N-1} \hat{C}_{n,m}\,u_m(\xi). \tag{14}$$

The eigenvalues and eigenfunctions in physical units are

$$E_n = \hbar\,\omega_0\,\tilde{E}_n \tag{15}$$

and

$$\Psi_n(x) = \sqrt{\alpha} \sum_{m=0}^{N-1} \hat{C}_{n,m}\,u_m(\alpha\,x). \tag{16}$$

The eigenfunctions are analytical functions whose derivatives are easily computed, so the accuracy can be checked by substitution in (5). As a rule of thumb, the last coefficients of each series $\{\hat{C}_{n,m}\}_{m=0}^{N-1}$ (say, the last 10 for $N = 60$) have to be very small.

The parameter ω_0 largely determines whether the truncated expansions of $\{\Psi_n\}$ are good approximations. As a rule of thumb the exponential in (10) should be small (say $\sim \mathrm{e}^{-2}$) at the estimated limits for the the particle position. This leads to $\omega_0 \approx 16\,\hbar/(m\,\Delta x^2)$, where Δx is the width of the classically allowed region, or $\tilde{\nu}_0 \approx 16/(m\alpha_0^2\Delta x^2)$ with $\tilde{\nu}_0$ and Δx in cm^{-1} and Å units, respectively. For a single minimum this is obtained if $\hbar\,\omega_0$ is close to the first observed transition. In this case, $N = 40$ is sufficient. For potentials composed of a narrow well and a shallow upper part it is necessary to increase the size to $N = 60$. The accuracy for the 10 lower eigenvalues is largely within experimental errors and the accuracy of the eigenvectors is better than 1%. Further increment of N is unnecessary as numerical errors increase for higher powers of x.

The INS intensity for a transition $|0\rangle \rightarrow |n\rangle$ at energy E_n is proportional to the scattering function[48]

$$S(Q, E) = |\langle n|\exp(-iQx)|0\rangle|^2\delta(E - E_n). \tag{17}$$

For a spectrometer like TFXA,[58] energy and momentum transfer, E and Q, respectively, are correlated as

$$E \approx 16.759 \times Q^2,$$

with E and Q in cm^{-1} and $\mathrm{\AA}^{-1}$ units, respectively.

---

† Electronic address: `fillaux@glvt-cnrs.fr`

‡ Electronic address: `cousson@llb.saclay.cea.fr`

§ Electronic address: `archilla@us.es`

¶ Electronic address: `J.Tomkinson@rl.ac.uk`

[1] G. Pimentel, C. McClellan, and A. Lester, *The hydrogen bond* (W.H. Freeman, San Francisco, 1960).

[2] S. N. Vinogradov and R. H. Linnell, *Hydrogen Bonding* (Van Nostrand-Reinhold, New York, 1971).

[3] P. Schuster, G. Zundel, and C. Sandorfy, *The hydrogen bond. Recent developments in theory and experiments*, vol. I, II and III (North-Holland Pub. Co., Amsterdam, 1976).

[4] G. A. Jeffrey and W. Saenger, *Hydrogen Bonding in Biological Structures* (Springer-Verlag, Berlin, 1991).

[5] S. Scheiner, *Hydrogen Bonding: A Theoretical Perspective* (Oxford University Press, Oxford, 1997).

[6] A. N. Baker Jr, J. Chem. Phys. **22**, 1625 (1954).

[7] M. Ichikawa, Acta Cryst. B **34**, 2074 (1978).

[8] P. Gilli, V. Bertolasi, V. Ferretti, and G. Gilli, J. Am. Chem. Soc. **116**, 909 (1994).

[9] V. Bertolasi, P. Gilli, V. Ferretti, and G. Gilli, Chem. Eur. J. **2**, 925 (1996).

[10] G. Gilli and P. Gilli, J. Molec. Struct. **552**, 1 (2000).

[11] J. A. Gerlt and P. G. Gassman, J. Am. Chem. Soc. **115**, 11552 (1993).

[12] M. M. Kreevoy and T. M. Liang, J. Am. Chem. Soc. **102**, 3315 (1980).

[13] W. W. Cleland, Biochemistry **31**, 317 (1992).

[14] W. W. Cleland and M. M. Kreevoy, Science **264**, 1887 (1994).

[15] P. A. Frey, S. A. Whitt, and J. B. Tobin, Science **264**, 1927 (1994).

[16] P. A. Frey, Magnetic Resonance in Chemistry **39**, S190 (2001).

[17] A. Warshel, A. Papazyan, and P. A. Kollman, Science **269**, 102 (1995).

[18] S. Scheiner and T. Kar, J. Am. Chem. Soc. **117**, 6970 (1995).

[19] A. Novak, Struct. and Bonding (Berlin) **18**, 177 (1974).

[20] B. Berglund and R. W. Vaughan, J. Chem. Phys. **73**, 2037 (1980).

[21] C. A. Klug, P. L. Lee, I.-S. H. Lee, M. M. Kreevoy, R. Yaris, and J. Schaefer, J. Phys. Chem. B **101**, 8086 (1997).

[22] J. A. Belot, J. Clark, J. A. Cowan, G. S. Harbison, A. I. Kolesnikov, Y.-S. Kye, A. J. Schultz, C. Silvernail, and X. Zhao, J. Phys. Chem. B **108**, 6922 (2004).

[23] S. X. Tian and H.-B. Li, J. Phys. Chem. A **111**, 4404 (2007).

[24] J. Sørensen, H. F. Clausen, R. D. Poulsen, J. Overgaard, and B. Schiott, J. Phys. Chem. A **111**, 345 (2007).

[25] S. F. Darlow and W. Cochram, Acta Cryst. **14**, 1250 (1961).

[26] S. F. Darlow, Acta Cryst. **14**, 1257 (1961).

[27] F. Fillaux, N. Leygue, J. Tomkinson, A. Cousson, and W. Paulus, Chem. Phys. **244**, 387 (1999).

[28] A. Novak, P. Saumagne, and L. D. C. Bock, J. Chim. Phys-Chim. Biol. **60**, 1385 (1963).

[29] F. Avbelj, B. Orel, M. Klanjsek, and D. Hadzi, Spectrochim. Acta **41 A**, 75 (1985).

[30] H. R. Zelsmann, Z. Mielke, and M. M. Ilczyszyn, Spectrochim. Acta **44 A**, 705 (1988).

[31] M. M. Ilczyszyn, J. Baran, H. Ratajczak, and A. J. Barnes, J. Mol. Struct. **270**, 499 (1992).

[32] J. Tomkinson, I. J. Braid, J. Howard, and T. C. Waddington, Chem. Phys. **64**, 151 (1982).

[33] J. Howard, J. Tomkinson, J. Eckert, J. A. Goldstone, and A. D. Taylor, J. Chem. Phys. **78**, 3150 (1983).

[34] J. Tomkinson, J. Penfold, and J. Howard, J. Mol. Struct. **142**, 1 (1986).

[35] N. Kalsbeek, K. Schaumburg, and S. Larsen, J. Molec. Struct. **299**, 155 (1993).

[36] A. Wong, K. J. Pike, R. Jenkins, G. J. Clarkson, T. Anupõld, A. P. Howes, D. H. G. Crout, A. Samoson, R. Dupree, and M. E. Smith, J. Phys. Chem. A **110**, 1824 (2006).

[37] M. Fukai, T. Matsuo, and H. Suga, K. Chem. Thermodynamics **20**, 1337 (1988).

[38] C. C. Wilson, L. H. Thomas, and C. A. Morrison, Chem. Phys. Letters **381**, 102 (2003).

[39] F. Fillaux, A. Cousson, and J. Tomkinson, Chem. Phys. Letters **399**, 289 (2004).

[40] P. George, C. W. Bock, and M. Trachtman, J. Phys. Chem. **87**, 1839 (1983).

[41] M. Garcia-Viloca, A. González-Lafont, and J. M. Lluch, J. Am. Chem. Soc. **119**, 1081 (1997).

[42] L. Golič and J. C. Speakman, J. Chem. Soc. pp. 2530–2542 (1965).

[43] D. Hadži, B. Orel, and A. Novak, Spectrochimica Acta **29A**, 1745 (1973).

[44] F. Fillaux and J. Tomkinson, Chem. Phys. **158**, 113 (1991).

[45] http://www-llb.cea.fr.

[46] P. W. Betteridge, J. R. Carruthers, R. I. Cooper, C. K. Prout, and D. J. Watkin, J. Appl. Cryst. **36**, 1487 (2003).

[47] http://www.xtl.ox.ac.uk/crystals.html.

[48] S. W. Lovesey, *Nuclear scattering, Theory of Neutron Scattered from Condensed Matter*, vol. I (Clarendon Press, Oxford, 1984).

[49] A. Witkowski, J. Chem. Phys. **47**, 3645 (1967).

[50] Y. Maréchal and A. Witkowski, J. Chem. Phys. **48**, 3697 (1968).

[51] S. F. Fischer, G. L. Hofacker, and M. A. Ratner, J. Chem. Phys. **52**, 1934 (1970).

[52] O. Henri-Rousseau and P. Blaise, *The infrared spectral density of weak hydrogen bonds within the linear response theory* (Wiley, New York, 1998), vol. 103, Edited by I. Prigogine and S.A. Rice of *Adv. Chem. Phys.*, p. 1.

[53] F. Fillaux, A. Cousson, and M. J. Gutmann, J. Phys.: Cond. Matter **18**, 3229 (2006).

[54] F. Fillaux, A. Cousson, and M. J. Gutmann, J. Phys.: Cond. Matter **20**, 015225 (2008).

[55] M. J. S. Dewar, E. G. Zoebisch, E. F. Healy, and J. J. P. Stewart, J. Am. Chem. Soc. **107**, 3902 (1985).

[56] E. Heilbronner, H. Rutishauser, and F. Gerson, Sch. Chem. G. **XLII-VII**, 2285 (1959).

[57] S. Y. Chan and D. Stelman, J. Chem. Phys. **39**, 545 (1963).

[58] http://www.isis.rl.ac.uk/molecularSpectroscopy/tfxa/.

TABLE I: Neutron single crystal diffraction data and structure refinement for potassium and cesium hydrogen bistrifluoroacetates. $\lambda = 0.8305$ Å. Space groups monoclinic $I2/a$ for potassium and $A2/a$ for cesium. Both with Z = 4. The criterion for used reflections was I $> 3\sigma$(I). The variance for the last digit is given in parentheses. In all cases, 76 parameters were used in refinement on F.

	$KH(CF_3COO)_2$		$CsH(CF_3COO)_2$	
	20K	298 K	14 K	298 K
a (Å)	8.68(1)	8.78(1)	13.44(1)	13.623(8)
b (Å)	10.023(9)	10.18(1)	4.942(9)	5.033(3)
c (Å)	9.146(9)	9.28(1)	14.35(1)	14.741(6)
β ($^\circ$)	100.36(8)	99.96(9)	112.88(9)	112.46(9)
V (Å^3)	782.6	817.0	878.4	934.0
D_x (Mg m^{-3})	2.259	2.164	2.722	2.559
Measured reflections	1979	2164	3476	3897
Independent reflections	1769	1472	1977	2096
Used reflections	1503	1142	1557	1062
R_{int}	0.037	0.038	0.048	0.064
R-factor	0.040	0.045	0.0399	0.043
Weighted R-factor	0.042	0.029	0.0345	0.040
Goodness of fit	1.070	1.088	1.049	1.079
Extinction coefficient	22.7(7)	17.2(8)	10.0(3)	11.2(9)

TABLE II: Atomic positions and isotropic temperature factors for $KH(CF_3COO)_2$ at 20 K (first lines) and 298 K (second lines). The variance for the last digit is given in parentheses.

Atom	x/a	y/b	z/c	U(iso)(Å^2)
K(1)	0.2500	0.47035(13)	1.0000	0.0022
	0.2500	0.4691(2)	1.0000	0.0306
C(1)	0.08108(6)	0.65992(5)	0.61071(5)	0.0020
	0.0771(1)	0.66238(9)	0.61201(9)	0.0306
C(2)	-0.04133(6)	0.66059(5)	0.71503(6)	0.0020
	-0.04356(9)	0.66241(8)	0.71512(8)	0.0260
O(1)	-0.02359(7)	0.58604(6)	0.82262(7)	0.0040
	-0.02706(13)	0.58871(11)	0.81966(11)	0.0333
O(2)	-0.15042(7)	0.74496(6)	0.67180(7)	0.0045
	-0.15011(14)	0.74556(14)	0.67428(14)	0.0426
F(1)	0.15118(7)	0.78039(7)	0.61351(7)	0.0050
	0.14415(18)	0.78021(15)	0.61321(18)	0.0519
F(2)	0.19203(7)	0.56895(7)	0.65128(7)	0.0046
	0.18745(15)	0.57426(17)	0.65321(17)	0.0490
F(3)	0.01440(8)	0.63619(7)	0.47010(7)	0.0046
	0.01325(19)	0.63720(16)	0.47512(13)	0.0474
H(1)	-0.2500	0.7500	0.7500	0.0166
	-0.2500	0.7500	0.7500	0.0574

TABLE III: Atomic positions and isotropic temperature factors for $CsH(CF_3COO)_2$ at 14 K (first lines) and 298 K (second lines). The variance for the last digit is given in parentheses.

Atom	x/a	y/b	z/c	U(iso)(Å^2)
Cs(1)	-0.2500	0.21541(18)	0.0000	0.0013
	-0.2500	0.2170(4)	0.0000	0.0377
F(1)	-0.01883(5)	0.61975(15)	0.15253(5)	0.0059
	-0.01376(14)	0.5971(4)	0.15586(14)	0.0652
F(2)	0.10983(5)	0.39738(15)	0.26553(5)	0.0069
	0.11435(18)	0.3806(5)	0.26110(12)	0.0761
F(3)	0.14684(5)	0.72718(14)	0.18559(5)	0.0063
	0.14651(17)	0.7048(4)	0.18308(15)	0.0722
O(1)	0.16871(5)	0.28677(13)	0.08444(5)	0.0050
	0.16517(9)	0.2837(3)	0.0796(1)	0.0445
O(2)	-0.00501(5)	0.18925(14)	0.05235(5)	0.0045
	-0.00336(8)	0.1803(3)	0.0543(1)	0.0442
C(1)	0.07995(4)	0.52050(11)	0.17554(4)	0.0031
	0.08238(8)	0.5005(2)	0.17453(7)	0.0401
C(2)	0.08431(4)	0.31424(11)	0.09597(4)	0.0027
	0.08415(6)	0.30433(18)	0.09498(7)	0.0312
H(1)	0.0000	0.0000	0.0000	0.0166
	0.0000	0.0000	0.0000	0.0592

TABLE IV: Thermal parameters in Å^2 units for $KH(CF_3COO)_2$ at 20 K (first lines) and 298 K (second lines). The variance for the last digit is given in parentheses. The thermal parameters account for the variation of the contribution of each atom to Bragg's peak intensities through the thermal factor T^{at} depending on the reciprocal lattice parameters a^*, b^*, c^*, and unit cell indexes in reciprocal space h, k, l, as $T^{at} = \exp[-2\pi^2(U_{11}^{at}h^2a^{*2} + U_{22}^{at}k^2b^{*2} + U_{33}^{at}l^2c^{*2} + 2U_{12}^{at}ha^*kb^* + 2U_{23}^{at}kb^*lc^* + U_{31}^{at}lc^*ha^*)]$.

Atom	U_{11}	U_{22}	U_{33}	U_{23}	U_{13}	U_{12}
K(1)	0.0027(4)	0.0018(4)	0.0020(4)	0.0000	0.0003(3)	0.0000
	0.035(1)	0.0263(8)	0.0325(9)	0.0000	0.0122(7)	0.0000
C(1)	0.00117(19)	0.00268(19)	0.0023(2)	0.00024(13)	0.00039(14)	0.00003(13)
	0.0297(4)	0.0329(4)	0.0299(3)	0.0029(3)	0.0078(3)	-0.0022(3)
C(2)	0.00157(19)	0.00238(19)	0.0023(2)	0.00055(14)	0.00060(14)	0.00064(13)
	0.0258(3)	0.0272(3)	0.0249(3)	0.0045(3)	0.0043(2)	0.0005(3)
O(1)	0.0038(2)	0.0048(2)	0.0035(2)	0.00241(17)	0.00120(17)	0.00108(15)
	0.0360(5)	0.0341(4)	0.0307(4)	0.0115(4)	0.0088(3)	0.0042(4)
O(2)	0.0033(2)	0.0060(2)	0.0047(2)	0.00268(17)	0.00194(17)	0.00312(16)
	0.0376(5)	0.0507(7)	0.0418(5)	0.0194(5)	0.0129(4)	0.0180(4)
F(1)	0.0049(2)	0.0048(2)	0.0054(2)	0.00042(18)	0.00072(18)	-0.00222(17)
	0.0523(8)	0.0457(7)	0.0597(8)	0.0074(6)	0.0150(6)	-0.0195(6)
F(2)	0.0027(2)	0.0054(2)	0.0057(2)	0.00058(18)	0.00076(18)	0.00219(17)
	0.0353(6)	0.0579(8)	0.0557(7)	0.0057(6)	0.0135(5)	0.0141(5)
F(3)	0.0054(2)	0.0057(2)	0.0025(2)	-0.00028(17)	0.00020(17)	-0.00006(17)
	0.0608(8)	0.0535(7)	0.0285(5)	-0.0032(5)	0.0094(5)	0.0005(6)
H(1)	0.0177(7)	0.0158(8)	0.0160(7)	0.0034(6)	0.0023(6)	0.0029(6)
	0.0539(17)	0.0577(18)	0.0582(17)	0.0199(15)	0.0034(13)	0.0152(14)

TABLE V: Thermal parameters in Å^2 units for $CsH(CF_3COO)_2$ at 14 K (first lines) and 298 K (second lines). The variance for the last digit is given in parentheses. See the caption of Table IV.

Atom	U_{11}	U_{22}	U_{33}	U_{23}	U_{13}	U_{12}
Cs(1)	0.0009(3)	0.0015(3)	0.0019(3)	0.0000	0.0009(2)	0.0000
	0.0319(6)	0.0359(7)	0.0526(9)	0.0000	0.0244(6)	0.0000
F(1)	0.0048(2)	0.0069(3)	0.0061(2)	-0.00185(18)	0.00239(17)	0.00167(19)
	0.0614(8)	0.069(1)	0.068(1)	-0.0250(8)	0.0275(7)	0.0110(8)
F(2)	0.0095(2)	0.0082(3)	0.0030(2)	0.00077(19)	0.00246(17)	0.0006(2)
	0.0959(13)	0.0907(14)	0.0369(7)	0.0065(8)	0.0199(8)	0.0014(12)
F(3)	0.0074(2)	0.0047(3)	0.0068(3)	-0.00216(19)	0.00288(18)	-0.00294(18)
	0.0837(12)	0.0581(9)	0.0777(12)	-0.0291(9)	0.0342(9)	-0.0324(9)
O(1)	0.0038(2)	0.0055(2)	0.0071(2)	-0.00185(18)	0.00373(16)	-0.00097(18)
	0.0344(5)	0.0458(6)	0.0592(7)	-0.0061(6)	0.0245(5)	-0.0035(5)
O(2)	0.0029(2)	0.0039(2)	0.0068(2)	-0.00313(18)	0.00219(16)	-0.00094(17)
	0.0305(4)	0.0407(6)	0.0634(7)	-0.0202(6)	0.0202(5)	-0.0076(4)
C(1)	0.00369(17)	0.0030(2)	0.00295(18)	-0.00084(14)	0.00151(13)	0.00004(15)
	0.0448(5)	0.0407(5)	0.0346(4)	-0.0067(4)	0.0148(3)	-0.0051(4)
C(2)	0.00267(18)	0.00290(19)	0.00315(18)	-0.00089(15)	0.00183(13)	-0.00025(14)
	0.0285(3)	0.0284(3)	0.0370(4)	-0.0012(3)	0.0130(3)	-0.0011(3)
H(1)	0.0131(6)	0.0176(8)	0.0185(7)	0.0006(7)	0.0053(5)	-0.0011(6)
	0.0403(13)	0.0498(16)	0.088(2)	-0.0059(17)	0.0247(14)	-0.0011(12)

TABLE VI: Gaussian decomposition of the INS spectra of $KH(CF_3COO)_2$ (KTFA) and $CsH(CF_3COO)_2$ (CTFA) in the OH stretching region (see Fig. 4). FWHM: full width at half maximum. IR: infrared. R: Raman.

Peak	Gravity center (cm^{-1})		FWHM (cm^{-1})		Area (%)		Observed
	KTFA	CTFA	KTFA	CTFA	KTFA	CTFA	
1	527	522	12	13	1.8	1.8	INS, R
2	559	550	29	24	2.7	1.8	INS, R, IR
3	601	596	20	22	4.5	4.2	INS
4	647	646	35	29	4.8	3.0	INS, R, IR
5	703	704	41	39	17.2	13.5	INS
6	747	749	17	28	1.9	4.4	INS, R, IR
7	792	797	61	59	29.9	30.6	INS
8	–	848	–	23	–	4.5	INS, R, IR
9	870	878	58	54	18.8	19.8	INS
10	942	949	95	72	16.8	14.3	INS
11	1038	1039	46	52	1.6	2.1	INS

TABLE VII: Observed and calculated OH stretching frequencies and INS relative intensities for $KH(CF_3COO)_2$ for the potential function $V = -185.074\,x + 122.598\,x^2 - 10.506\,x^3 - 1232.04\exp(-28.149\,x^2)$. V and x are in $cm^{-1}$and Å units, respectively.

Transitions	Observation			Grouping	Calculation		
	$h\nu$	Q	Int.		$h\nu$	Q	Int.
	(cm^{-1})	($Å^{-1}$)	(au)		(cm^{-1})	($Å^{-1}$)	(au)
$0 \rightarrow 1$	601	6.0	0.30	1+2+3	614	6.1	0.38
$0 \rightarrow 2$	703	6.5	0.80	4+5+6	701	6.5	0.93
$0 \rightarrow 3$	792	6.9	1.00	7	787	6.9	1.00
$0 \rightarrow 4$	870	7.2	0.63	8	872	7.2	0.59
$0 \rightarrow 5$	942	7.6	0.56	9	953	7.5	0.37

Figure captions

FIG. 1: (Color online) Potential function, eigen states and wave functions along the stretching coordinate of the hydrogen bond proton in potassium hydrogen maleate, after Ref. [27].

FIG. 2: (Color online) Comparison of the hydrogen bistrifluoroacetate entities of the potassium salt at 20 K and 300 K. Right: projection onto the mean-plane of the carboxylic entities. Left: view along the hydrogen bond direction. The ellipsoids correspond to 50% probabilities for atoms.

FIG. 3: (Color online) Comparison of the hydrogen bistrifluoroacetate entities of the cesium salt at 14 K and 300 K. Right: projection onto the mean-plane of the carboxylic entities. Left: view along the hydrogen bond direction. The ellipsoids correspond to 50% probabilities for atoms.

FIG. 4: Inelastic neutron scattering spectra and band decomposition into gaussian profiles in the ν_a region for $KH(CF_3COO)_2$ and $CsH(CF_3COO)_2$ at 20 K. Only the filled components have counterparts in Raman (see text). The residual of the fit is compared to error bars.

FIG. 5: (Color online) Left: Calculated potential and energy levels for $KH(CF_3COO)_2$. $V = -185.074\,x + 122.598\,x^2 - 10.506\,x^3 - 1232.04\exp(-28.149\,x^2)$, with V and x in cm^{-1} and Å units, respectively. Right: Calculated wave functions.

FIG. 6: Schematic representations of strong symmetric hydrogen bonds in trifluoroacetate dimers (top) and hydrogen maleate (bottom), in the ground state (left) and in excited vibrational states (right). The wedge bonds represent lone pair orbitals (see text).

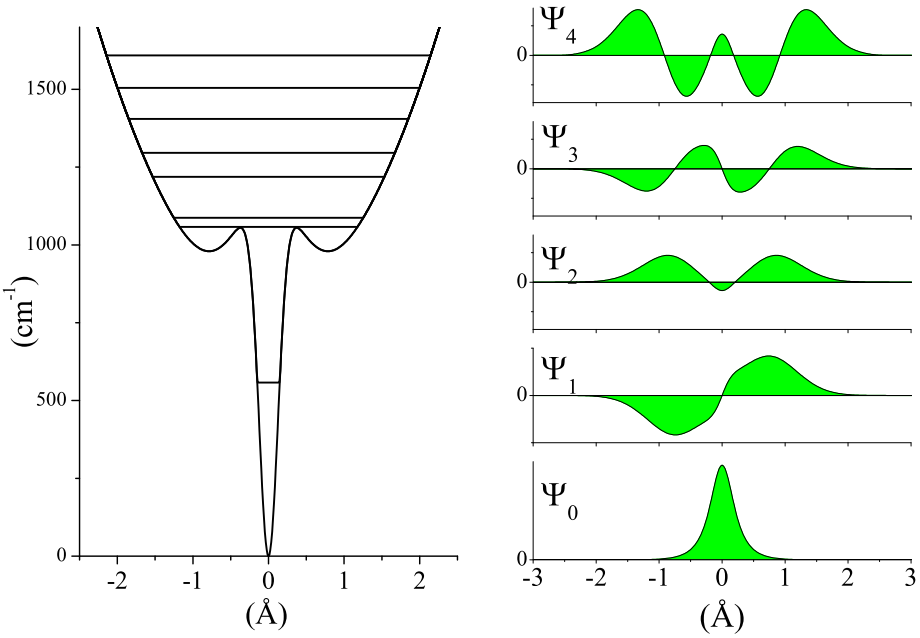

FIG. 1:

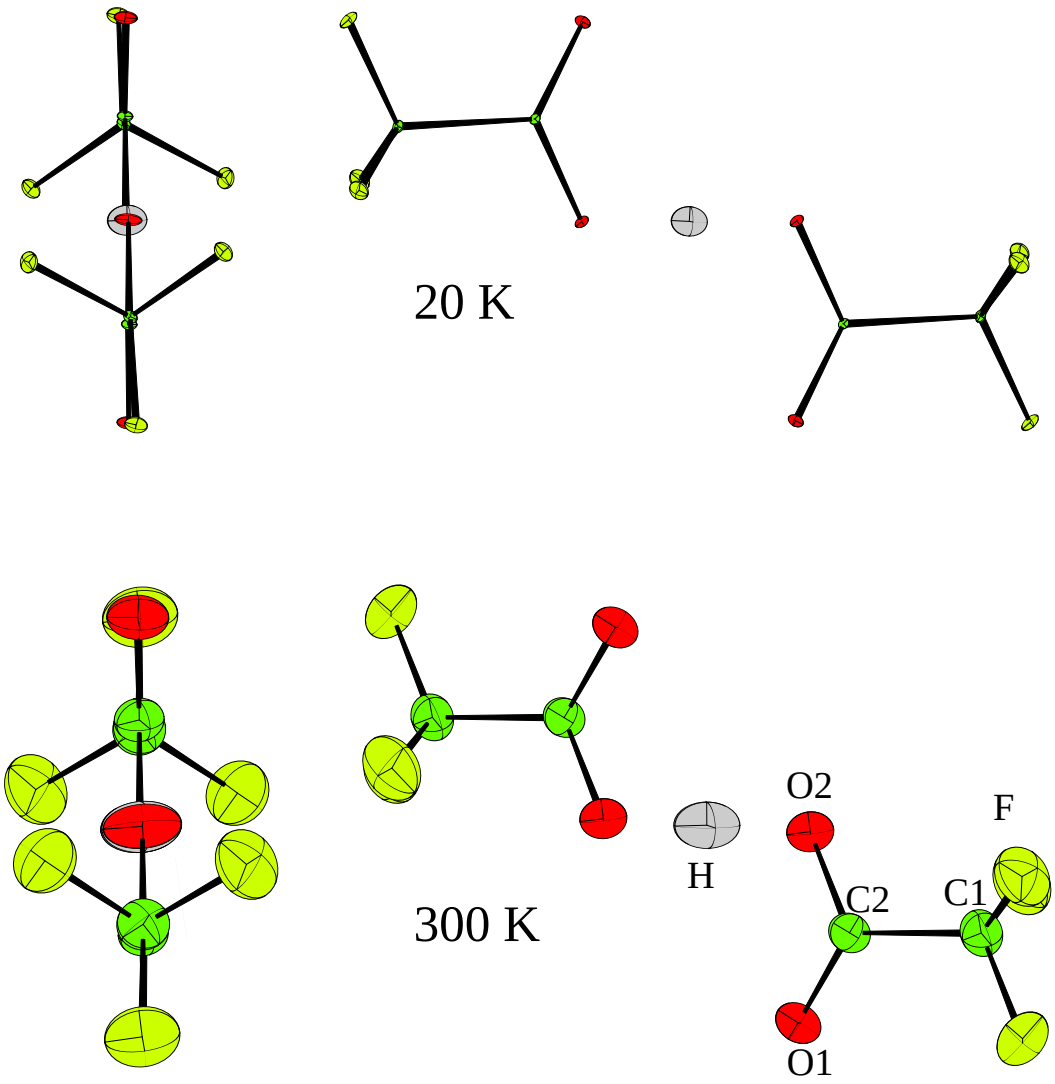

FIG. 2:

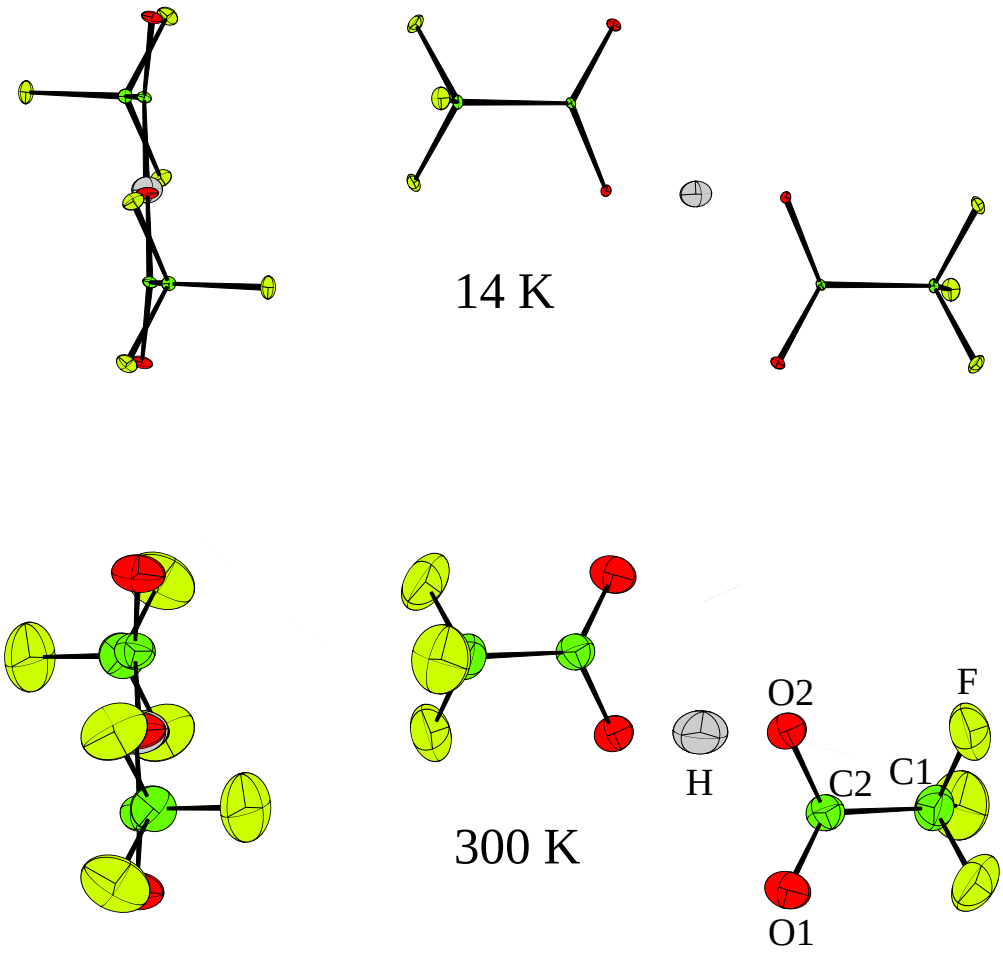

FIG. 3:

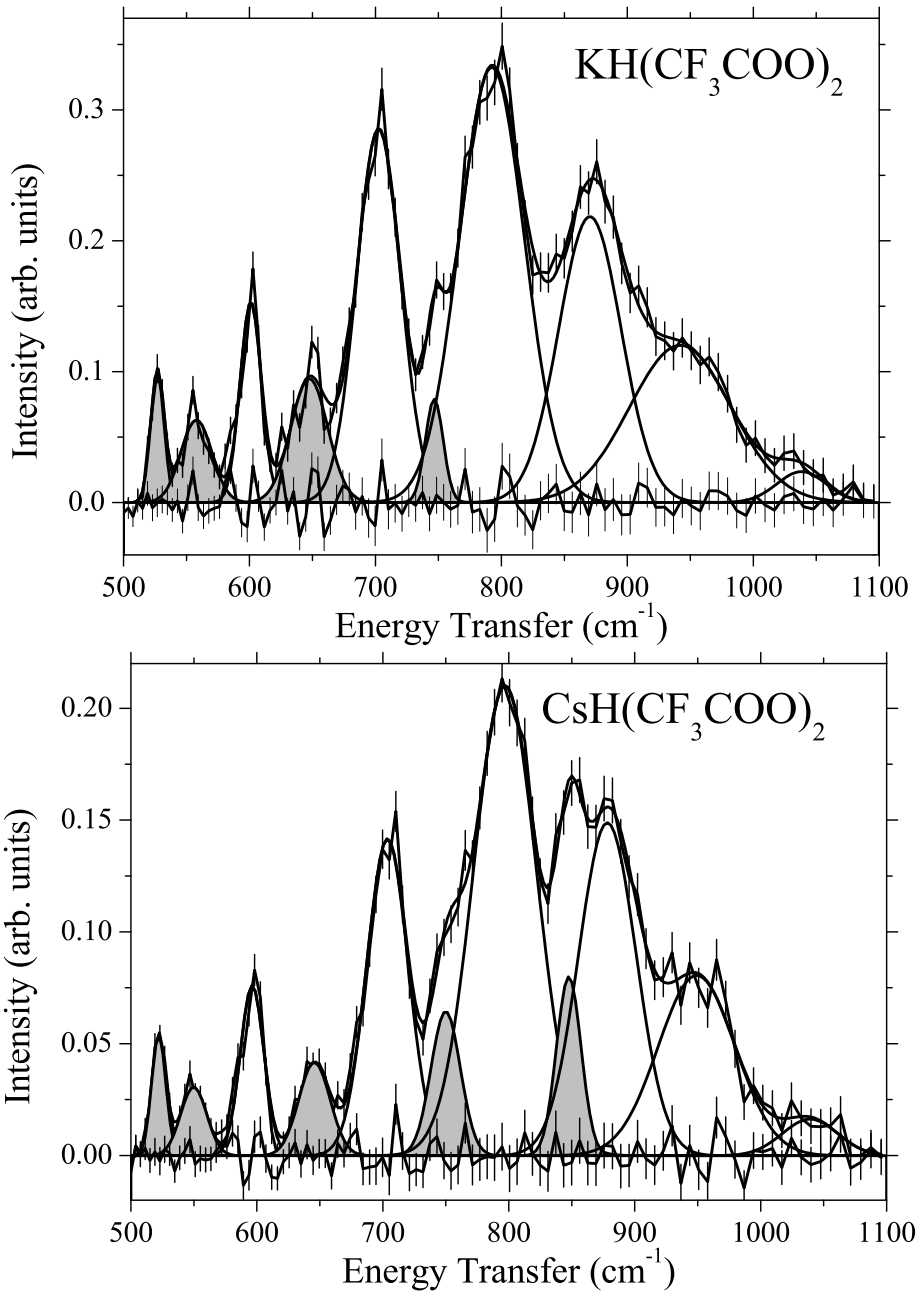
KH(CF3COO)2
Intensity (arb. units)
0.0
0.1
0.2
0.3
500
600
700
800
900
1000
1100
Energy Transfer (cm-1)
CsH(CF3COO)2
Intensity (arb. units)
0.00
0.05
0.10
0.15
0.20
500
600
700
800
900
1000
1100
Energy Transfer (cm-1)

FIG. 4:

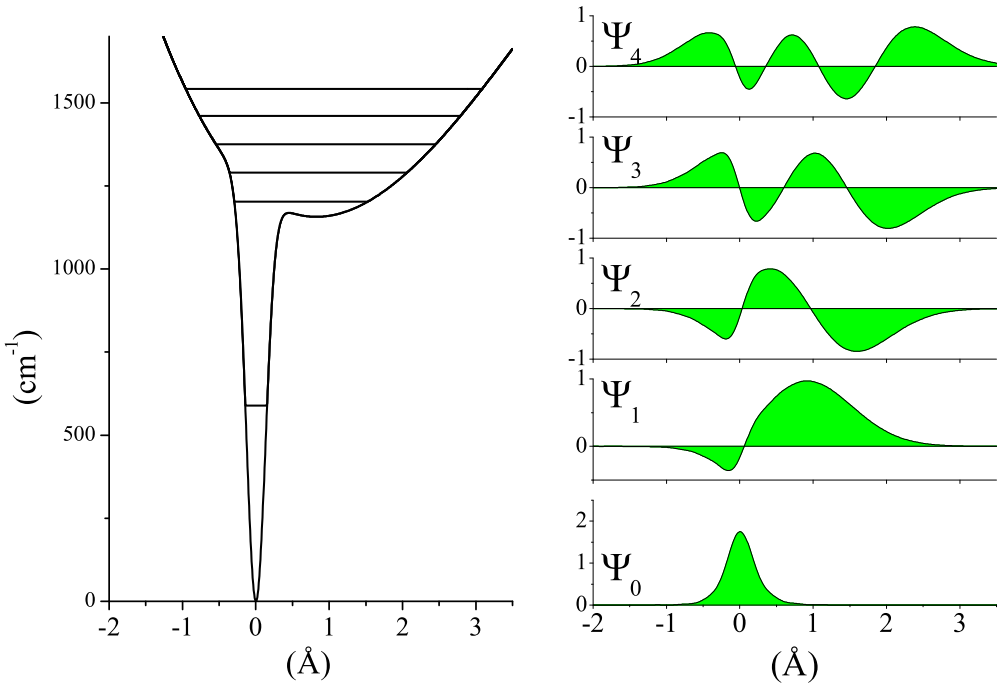

FIG. 5:

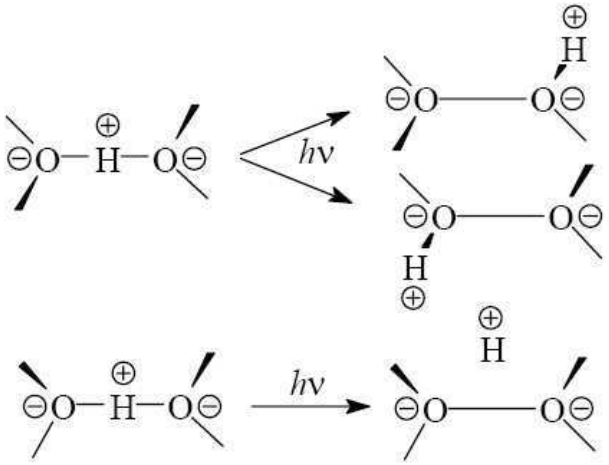

FIG. 6: